https://doi.org/10.1016/j.enbuild.2021.111393

An experimental study of condensation on an aluminum radiant ceiling panel surface with superhydrophobic treatment

Ziwen Zhong[1], Jianlei Niu[1,*], Wei Ma[2], Shuhuai Yao[2], Meng Yang[3], Zuankai Wang[3]

[1] Department of Building Services Engineering, The Hong Kong Polytechnic University, Hong Kong, China

[2] Department of Mechanical Engineering, The Hong Kong University of Science and Technology, Hong Kong, China

[3] Department of Mechanical Engineering, City University of Hong Kong, Hong Kong, China

*Corresponding author: email: jian-lei.niu@polyu.edu.hk

Key words: superhydrophobic, condensation, cooled-ceiling panels, water self-repellency

Abstract

One of the factors that limit the cooling capacities and application potentials of radiant cooling panels is the condensation risk. The self-condensate-repellency tendency of superhydrophobic surface materials provides a possibility to mitigate the condensation risk. This paper studied the size ranges of condensate drops formed on a superhydrophobic aluminum sheet of the size 25 mm x 25 mm attached to a cooled ceiling panel in a climate chamber in the humidity range between 50% and 80% and at the temperature of 25°C and air change rates from 0 ACH to 9 ACH. Using an optical magnifier, large drops up to the size 802.5 μm were observed in certain fixed positions in the large view area of 4.08 mm x 3.06 mm under different experimental conditions; whereas in a smaller focused view area of 0.96 mm x 0.72 mm the diameters of the largest drops were found to firstly increase over time and then reached around 80 μm with occasional size of 152 μm. All these were in contrast with the continuously growing drops simultaneously observed on the ordinary aluminum sheet, which reached 4 mm. The largest size of the droplets in the small focused area increased from 54.1 μm to 151.7 μm as humidity increases from 50% to 80%, but did not change much as the air change rate changed from 0 ACH to 9 ACH. This series of experiments confirm our hypothesis that condensate drop sizes can be limited within the un-

perceivable range, namely below the sensory and visual thresholds, in typical indoor conditions because of the droplet jumping mechanism that occurs on the nano-engineered superhydrophobic surface, but it remains to be ascertained whether the large condensate drops formed at certain fixed points in the other parts of the tested nanostructured surface were associated with some defects in the nano-scale, and this can be eliminated via on a larger area of practical applications.

1 Introduction

Buildings consume more than 90% of electricity in Hong Kong [1], and air-conditioning systems contribute to a share of 30% of energy consumption in these buildings [2]. With the accelerating global warming [3], the dependence on air-conditioning will further increase energy consumption to cope with the increased frequency, intensity, and duration of extreme heat exposure [4]. As one of the alternatives to air-conditioning technology, radiant cooling systems have merits of energy saving, quiet operation, high thermal comfort level [5, 6], but its application is limited due to the condensation risk. To avoid condensation, indoor humidity and the radiant cooling surface temperature must be carefully controlled [5]. Mumma [7-9] introduced dedicated outdoor air systems (DOAs) to be integrated with ceiling radiant cooling panels to control indoor humidity. Niu and Zhang [10, 11] estimated the system performances when a desiccant dehumidification system is combined with radiant cooling systems to realize the temperature and humidity independent control. Despite the necessary dehumidification [12-14], the temperature of radiant cooling surfaces should be strictly controlled at a safety margin of 1-2 K above the indoor air dew point to tolerate the variation of indoor humidity [15, 16]. However, dehumidification systems can not handle sudden rises of humidity, say, the opening of windows, and also the cooling capacity is limited due to the raised chilled water temperature. In addition to the air humidity control, novel radiant cooling panels combined with cooled liquid desiccant and membrane [17-19] and hydronic cooling panels covered with membrane transparent to long-wave thermal radiation [20-22] have also been proposed.

Cooled ceiling panels are usually made of hydrophilic white-painted galvanized steel sheets or aluminum sheets, on which film condensation is the main regime. People's concern on condensation mainly originates from the risk of gravity-induced dripping of large droplets formed from the condensate water film on the ceiling panel. Different to hydrophilic surfaces, superhydrophobic surface is characteristic that the contact angle (CA) of the surface is higher than 150^{o} and the contact angle hysteresis (CAH) is ultra low (usually lower than 10^{o}) [23, 24]. Previous studies have reported that condensate droplets formed on some superhydrophobic surfaces would detach from the surface spontaneously when they reached the scale below a few hundred microns [25-31]. Boreyko and Chen [28] observed that this was caused by the jumping motion in the out-of-plane behavior of tiny condensate drops on the superhydrophobic surface. The jumping motion was triggered by the excess surface energy released through the coalescence of drops. Chen et.al [27] performed a one-hour condensation experiment using a superhydrophobic silicon substrate in the ambient environment and found that condensate drops nucleated, grew, and disappeared with an average diameter of 50 μm on the superhydrophobic surface periodically. Thus, the condensation regime on some superhydrophobic surfaces provides a possibility for mitigating condensation risks of radiant cooling systems. Tang et.al [32] explored the concept by studying the size of condensate drops on a superhydrophobic copper sheet. The measured apparent CA, receding CA, and advancing CA of the superhydrophobic copper sheet were 161.6^{o}, 120.4^{o}, and 170.6^{o}, and the contact angle hysteresis was 50.2^{o}. The material was attached to a cooled copper panel and placed in the air of the temperature of 30^{o}C and humidity of 50% RH for 24 hours, and it was found that 90% of the coalescence-induced departure drops had a radius smaller than 300 μm, which is comparable to people's sensory threshold, which was concluded from a tactile stimuli investigation containing 30 subjects. Continuous growth of anchored drops with a radius reaching 700 - 1000 μm was observed on the superhydrophobic copper sheet, which is possibly related to the intrinsic characteristics of the surface.

The concept of using superhydrophobic surfaces to mitigate condensation risks of cooled ceiling panels relies on the hypothesis that the condensate droplet size can be constrained within the perceptional threshold of people through the jumping condensation mechanism in a longtime operation. To date,

however, there has been no experimental observation on the continuous condensation behavior of tiny droplets formed on a superhydrophobic surface under a longtime condensation in typical indoor conditions. Besides, the relationship between the condensate drop size on superhydrophobic surfaces and the indoor humidity and air change rates has not been studied yet.

In this study, we attempt to explore if the desirable hydrophobic surfaces can be produced on the commonly used radiant ceiling panel material aluminum and whether the self-jumping phenomenon of the condensate drops will occur in a realistic radiant-panel installation. We also aim to see how the sub-cooling degree, i.e., the panel surface temperature below the room dew-point temperature, may affect the actual condensate drop sizes formed on the surface.

2 Methods

2.1 Material fabrication

The superhydrophobic aluminum sheet was prepared through the following fabrication procedures [33]. Pure aluminum (purity: 99.99%) with 0.2mm thickness was used as substrate. The aluminum foil was cleaned by sonication in acetone for 5 min, followed by an equal-time sonication in Isopropyl alcohol (IPA) and deionized (DI) water successively. The sample was immersed in 80℃ 0.05M NaOH solution to form microstructures by chemical etching method. Then, after heating in water bath at 90℃ for an hour, the fluorination treatment in 0.5%wt 1H,1H,2H,2H perfluorodecyltriethoxysilane (FAS-17)/hexane solution was conducted after 30 min drying at 120℃. The topographies of the superhydrophobic surface were analyzed with scanning electron microscopy (SEM, JEOL-6390). The contact angle and contact angle hysteresis was measured using 5μl water droplets on Station Contact angle meter (Biolin Theta).

2.2 Experimental setup

The schematic and the photograph of the experimental setup are shown in Fig.1 and Fig. 2 respectively. The condensation experiment was performed in a climate chamber (length 4 m, width 2.7 m, height 2.9 m) equipped with a primary air unit (PAU). The flow rate and temperature of supply air can be controlled

through the controller of the PAU. An electric radiation heater and a humidifier were placed inside the chamber to control the indoor temperature and humidity. A hydronic cooled ceiling panel (SAS International) with a size of 1.2 m x 0.6 m was mounted in the chamber and was connected with a water chiller through copper pipes. Two pure aluminum sheets and two superhydrophobic aluminum sheets, both with a size of 2.5 cm x 2.5 cm, were affixed on the panel using silicone thermal grease (ShinEtsu X23-7868-2D). One sheet was used as the testing sample, and the other was used as the blank sample to measure the surface temperature, as shown in Fig. 2.

T-type thermocouples (KAIPUSEN SA1TTT30SLE) were attached to the blank superhydrophobic sample (T101) and the blank aluminum sample (T102) and the panel surface (T103), as shown in Fig. 2. The temperature of the blank samples was used to represent the temperature of the testing samples. The data was recorded by a thermocouple data logger (DL). The temperature of the supply chilled water, return chilled water, and panel surface was measured through three-wire RTDs. The flow rate of chilled water was measured through a water flow sensor (WFS). Two temperature and humidity transmitters H1 and H2 (HOBO U12-011) were used to measure the air temperature and humidity in the upper zone and lower zone of the chamber respectively. The temperature and humidity of supply air and return air was measured by duct-mounted humidity transmitters (VAISALA HMD65). The data of RTDs, WFS, and the duct-mounted humidity transmitters (DH) was recorded and uploaded to the computer by a remote data acquisition system (DAQ).

The image of the condensate on the superhydrophobic aluminum sheet was captured by a digital camera (UCMOS05100KPA) with a zoom lens (FT-OPTO FB065). An electric stack rail was used to adjust the distance between the lens and the testing samples to focus on the condensate drops in the experiment. The image of condensate on the pure aluminum sheet was also captured using a digital camera (Supereyes). Both the two digital cameras were mounted on an aluminum extrusion frame placed in the chamber.

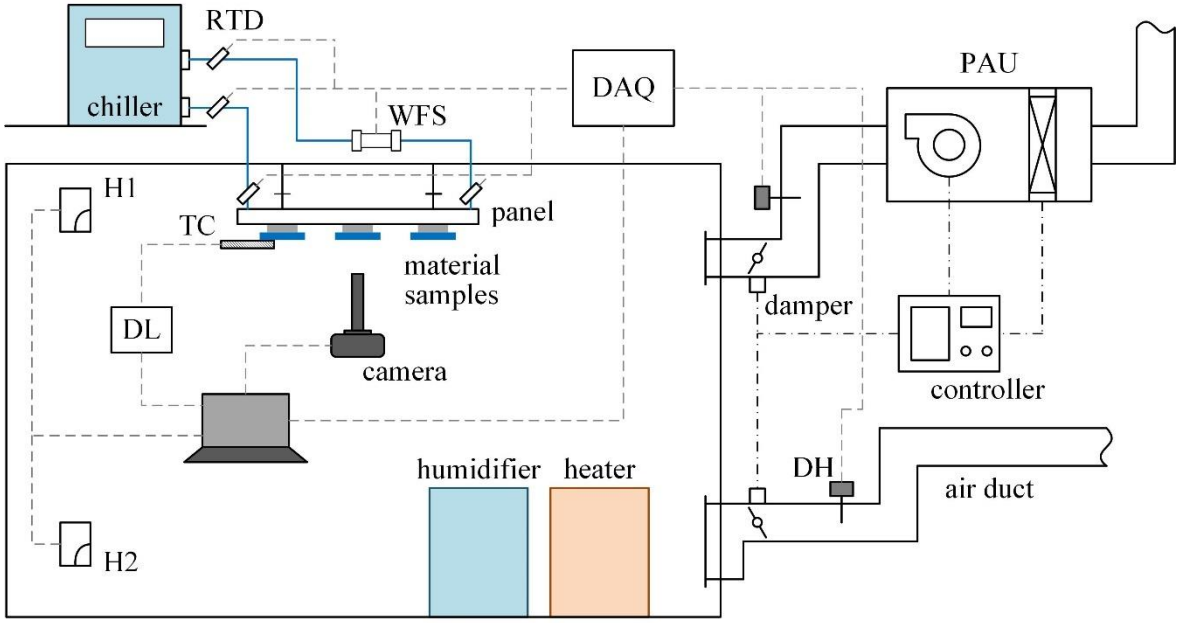

Fig. 1. The schematic of the experimental setup.

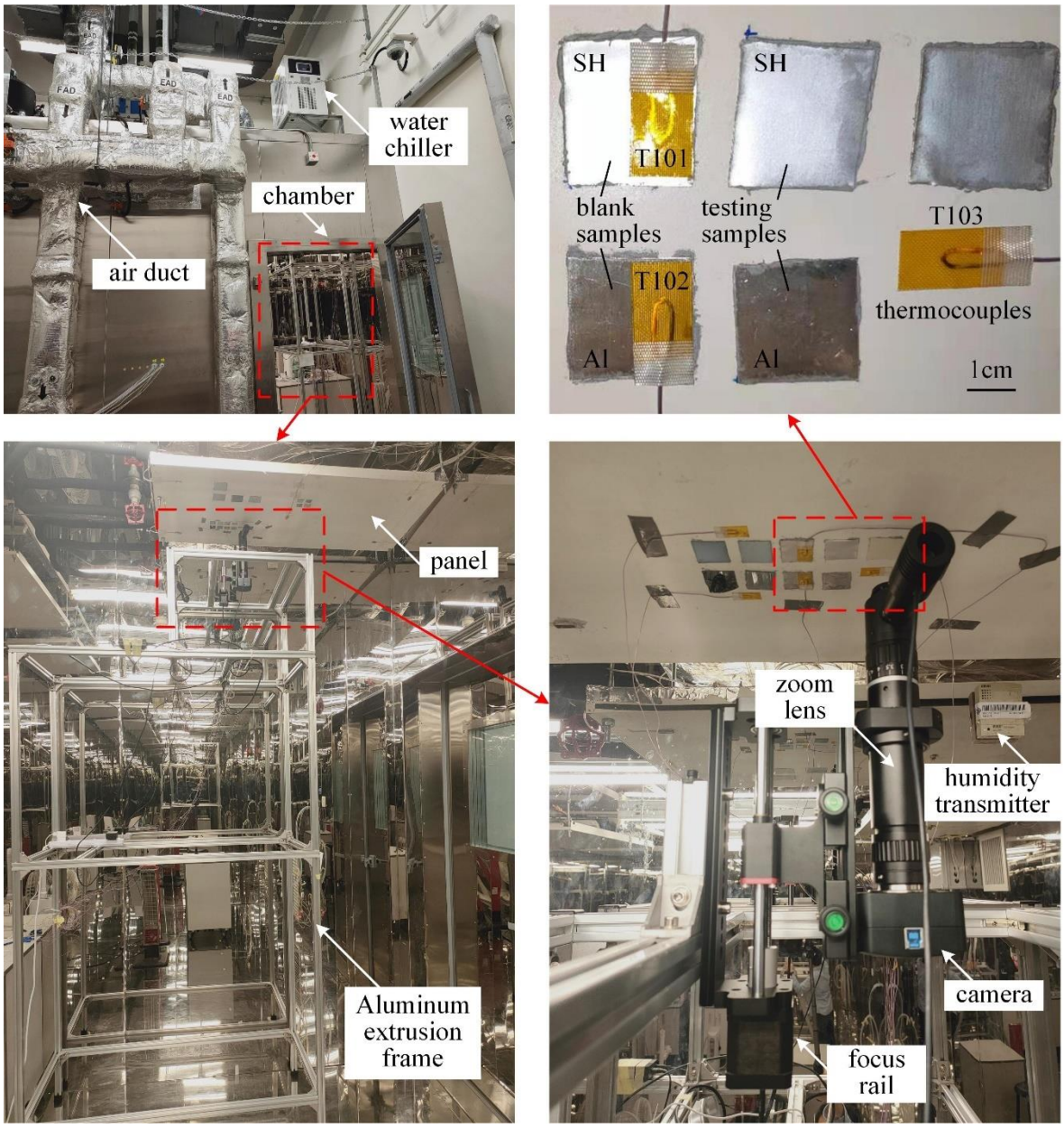

Fig. 2. The photograph of the experimental setup.

2.3 Experimental procedures

The experiment was performed under various relative humidity between 50% and 80% at the temperature of 25°C and various air change rates between 0 ACH and 9 ACH at the temperature of 25°C and humidity of 60%. The experimental conditions are listed in Table 1. It should be noted that condition A2 and B1 are same experimental set but with different labels. The hydronic radiant ceiling panel was cooled by chilled water of 6°C. The water flow rate was maintained at 20 L/min to narrow the temperature difference of the supply and return water.

Table 1

Experimental conditions.

	Chamber Indoor Air			Chilled Water	
Condition No.	Air change rates	Temperature (°C)	RH (%)	Temperature (°C)	Flow rate (L/min)
A1	0	25	50	6	20
A2	0	25	60	6	20
A3	0	25	70	6	20
A4	0	25	80	6	20
B1	0	25	60	6	20
B2	3	25	60	6	20
B3	6	25	60	6	20
B4	9	25	60	6	20

To carry out the experiment, the samples were affixed onto the cooled ceiling panel firstly. Then, the thermocouples, the humidity transmitters, and the camera were mounted at predetermined positions. The water chiller was launched after the indoor temperature and humidity and air change rates were controlled to the expected level. Each condition was maintained for eight hours to simulate a normal working period in offices, starting from the time when condensation occurs on the samples. To observe condensate drops with a size range of 10 μm - 1000 μm on the superhydrophobic aluminum sheet, the image of condensate in two different focused areas, the large view area V1 (4.08 mm x 3.06 mm) and the small view area V2 (0.96 mm x 0.72 mm), was captured by using different magnification scales of the zoom lens. After the experiment, the condensate picture of all samples was taken using a smartphone camera. The experimental procedures and the picture sample of different focused areas are shown in Fig. 3. The view area V1 is a small part of the testing superhydrophobic sample, and similarly, the view area V2 is a small part in the center of the view area V2.

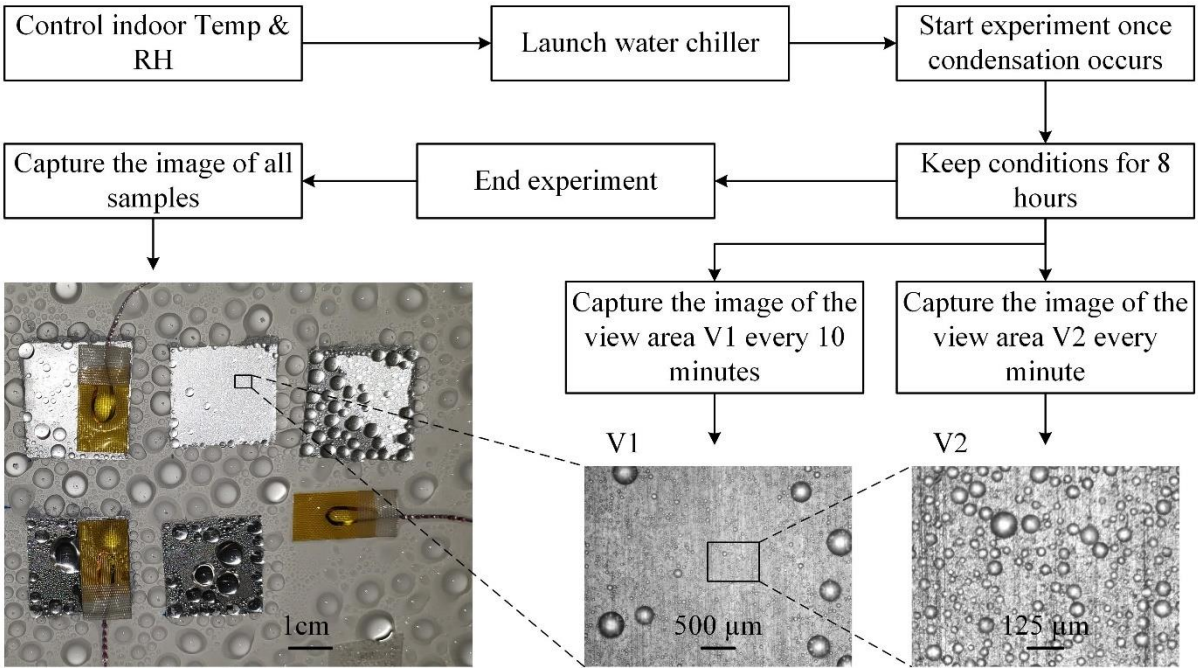

Fig. 3. The experimental procedures and picture samples of different focused areas.

2.4 Image processing

The size of condensate drops was obtained by analyzing condensate images. The image processing software Fiji [34] and the machine learning based Trainable Weka Segmentation tool [35] was used to analyze images.

2.5 Error analysis

Two parts of errors were considered in this study. First, the measurement error of temperature and humidity and flow rate is related to the accuracy of sensors listed in table 2. The second part is the measurement error of droplet size in image analysis. A micro-ruler with a division of 0.5 mm was used to measure the length and width of the camera view. To reduce the error in determining the length scale, the length between the same side of ruler ticks was measured for ten times and the average was used. For the droplet diameter obtained from condensate images, 1 to 2 pixels of error may be contained in measurements, which may result in a relative error of 0.25% - 10% depending on the droplet size in terms of pixels.

Table 2

Accuracy of sensors.

Sensors	Accuracy
Thermocouples	0.5 °C
RTDs	0.2 °C
Room temperature/humidity transmitter	Temperature: ±0.35 °C Humidity: ±2.5%
Duct-mounted temperature/humidity transmitter	Temperature: ±0.1 °C Humidity: ±1.5%
Water flow sensor	±0.5% F.S.

3 Results

3.1 Material analysis

As shown in Fig. 4(a), micro-bumps with diameters of 1.5 μm - 2.5 μm were formed on the superhydrophobic aluminum sheet. Nano-flowers can be seen on the micro-bumps shown in Fig. 4(b). The aluminum substrate was functionalized with superhydrophobicity by fluoridation on hierarchical structures. The measured contact angle of the superhydrophobic aluminum sheet is 169°, and the contact angle hysteresis is less than 5°.

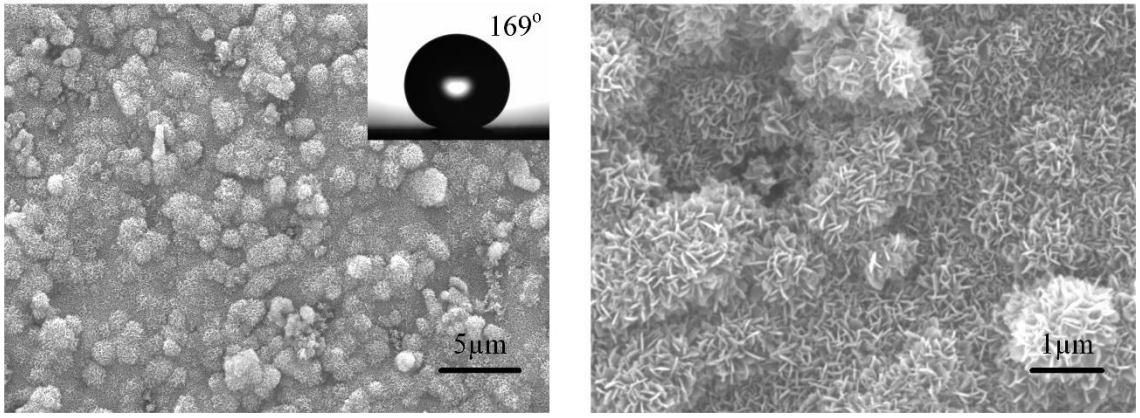

Fig. 4. The SEM image of the superhydrophobic aluminum sheet.

3.2 Indoor air conditions and sample surface temperature

The air change rates (ACH) in the chamber, the air temperature (Temp) and relative humidity (RH) in the ceiling area, and the temperature of blank samples (T101, T102) and the panel surface (T103) under

each condition are listed in table 3. The air dew point (DPT) is calculated from the measured air temperature and relative humidity. The subcooling degree is defined as the difference between the air dew point and the average of T101 and T102.

Table 3

The air change rates, the air temperature and relative humidity in the ceiling area, and the temperature of blank samples and the panel surface.

		Ceiling area			Blank samples		Panel	Sub-cooling (ºC)
Condition No.	ACH	Temp (ºC)	RH (%)	DPT (ºC)	T101 (ºC)	T102 (ºC)	T103 (ºC)	
A1	0	25.1	50.6	14.2	11.4	11.4	11.5	2.8
A2	0	25.1	60.2	16.8	12.3	12.4	12.5	4.5
A3	0	25.1	69.9	19.2	13.0	12.9	13.0	6.2
A4	0	25.1	79.9	21.4	13.5	13.4	13.4	7.9
B1	0	25.1	60.2	16.8	12.3	12.4	12.5	4.5
B2	3.1	25.0	60.0	16.7	12.3	12.4	12.6	4.4
B3	5.9	25.1	60.2	16.8	12.2	12.4	12.5	4.6
B4	9	25.1	60.1	16.8	12.3	12.4	12.6	4.5

3.3 Condensate on the superhydrophobic aluminum sheet under various indoor humidity

3.3.1 Condensate in the large view

The condensate image of the view area V1 under the experimental condition A1 - A4 is shown in Fig. 5. In the case of condition A4 shown in Fig. 5(d), the condensate image at 3h50min instead of 5h was presented to include as many droplets as possible in the view area. A comparison of condensate under different conditions shows that more large drops are more likely to appear under higher humidity. Another interesting and important finding is that some large drops which are significantly larger than surrounding droplets always appear in certain fixed positions in different experimental conditions. These positions which include the top left, bottom left, top right, and bottom right of the view area are highlighted by the ellipses shown in Fig. 5(b) – (c). The formation of large drops in fixed positions is likely to be related to the local microstructures of the superhydrophobic surface, which will be discussed in the discussion section.

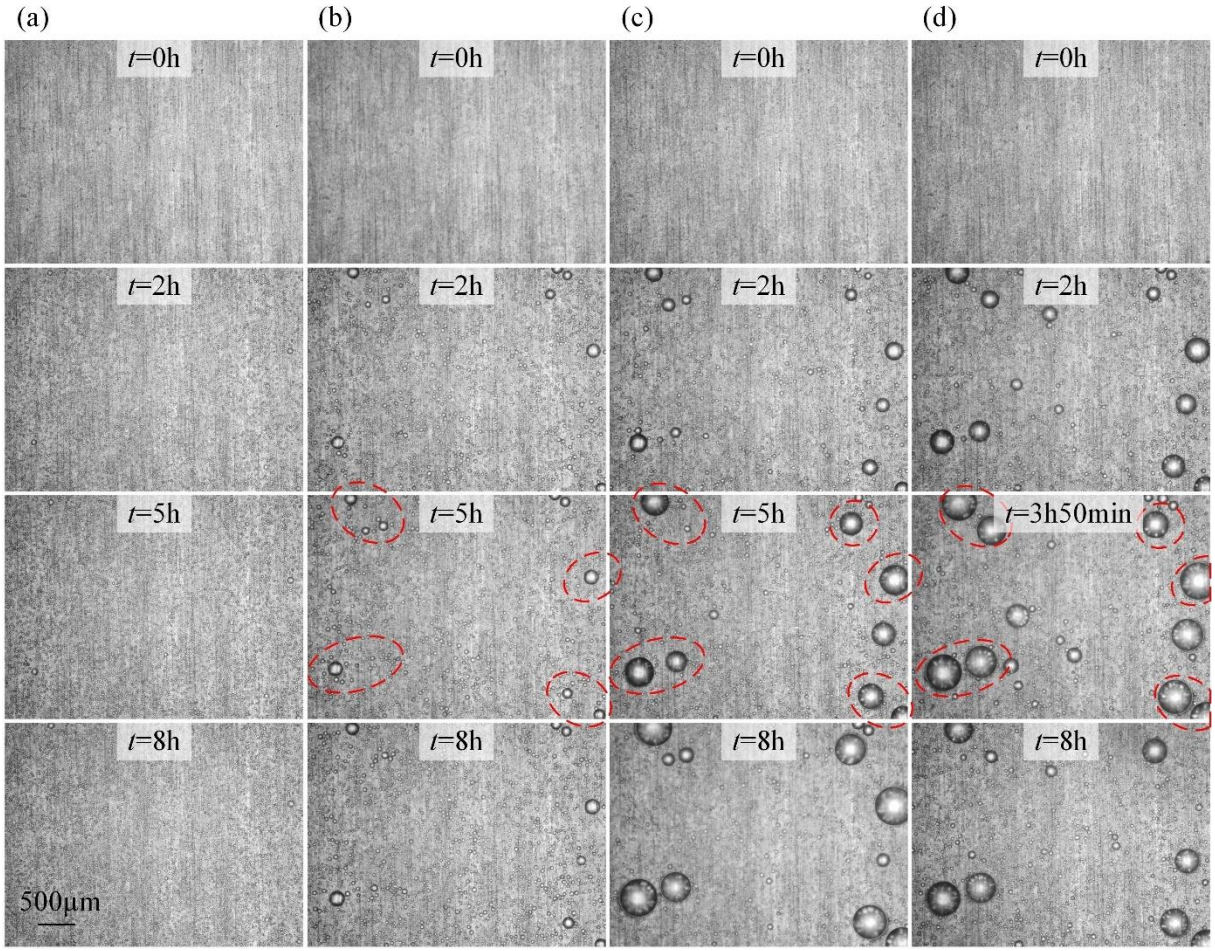

Fig. 5. The condensate image of the view area V1 under various indoor humidity: (a) 25ºC, 50%RH. (b) 25ºC, 60%RH. (c) 25ºC, 70%RH. (d) 25ºC, 80%RH.

The difference of condensate distributed in other positions like the central area is not so obvious compared with the positions where there are large drops. To further observe tiny droplets in the central area, the condensate of the view area V2 was observed by adjusting the magnification scale of the zoom lens.

3.3.2 Condensate in the small view

Fig. 6 shows the condensate image of the view area V2 under the experimental condition A1 – A4. Compared with the view area V1, the difference of the condensate droplet size distribution of the view area V2 was relatively small, and there were no droplets that are significantly larger than the surrounding droplets as in the view area V1. In the case of condition A1, the average droplet size is smaller than that

of higher humidity. The droplet size distribution is not much different under the humidity between 60% RH and 80% RH. More importantly, the droplet size distribution of the view area V2 did not change much with time but seemed to reach a steady state during 8-hour experiments. This is in line with our hypothesis for using superhydrophobic materials to mitigate condensation risks of cooled ceiling panels, that is, the condensate droplets on the superhydrophobic surface can be limited to a certain size range rather than growing continuously and eventually forming large droplets.

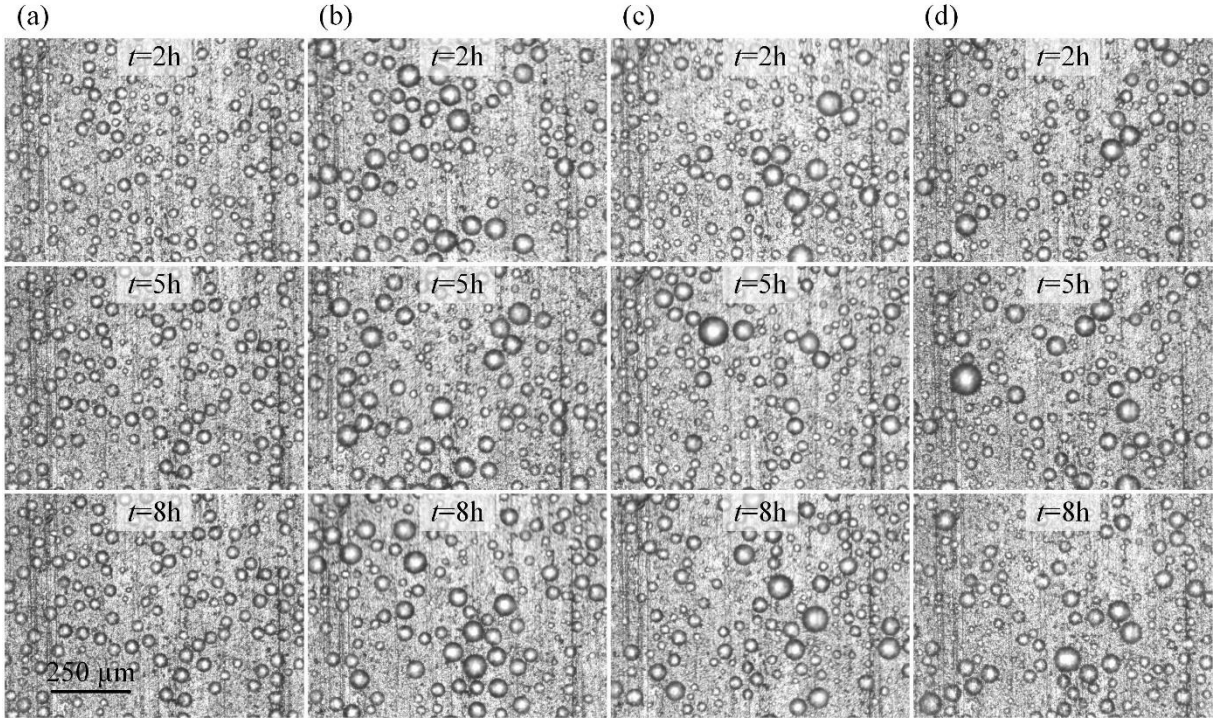

Fig. 6. The condensate image of the view area V2 under various indoor humidity: (a) 25ºC, 50%RH. (b) 25ºC, 60%RH. (c) 25ºC, 70%RH. (d) 25ºC, 80%RH.

The constrained droplet size can be explained by the jumping condensation mechanism. Fig. 7 shows the condensate image of the view area V2 at a certain time under condition A4. Four groups of droplets circled by dashed ellipses at the time of 18min, which may contain two, three, or four droplets, disappeared from the view one minute later. Similarly, six groups of droplets containing two or three droplets at the time of 7h53min disappeared from the view one minute later. It can be seen that a droplet always disappeared together with its neighboring droplets. The diameter of the disappeared droplets is between 30 μm and 80 μm, which is two orders of magnitude smaller than the capillary length of water. The group behavior of the disappearance of droplets and the size range of the disappeared droplets

indicated that the detachment of tiny droplets was very likely to be triggered by the coalescence-induced jumping motion [26-28]. Since the behavior can been observed from the early stage to the late stage of the experiment, the detachment of condensate droplets was proved to continuously occur during the whole experiment. This is in line with our hypothesis that the jumping condensation on the superhydrophobic surface can last over a long period of time.

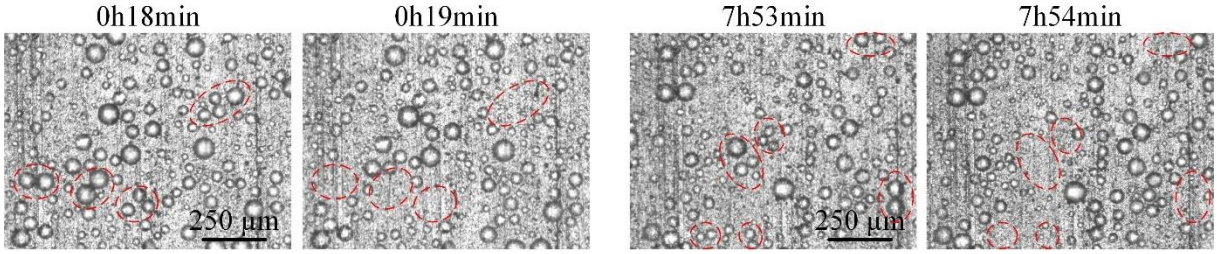

Fig. 7. Coalescence-induced detachment of groups of condensate droplets.

There were 480 condensate images of V2 captured in experiments for each condition. We analyzed the diameter of the largest droplet in every image (hereafter referred to as the maximum diameter) and use the maximum diameter as an index to investigate the relationship between the condensate droplet size and indoor humidity. Fig. 8(a) shows the curve of the maximum diameter changing over condensation time under condition A1 – A4. The maximum diameter under the humidity condition of 50% RH keeps stable around 50 μm after 3-hour condensation, but for the humidity condition of 60% - 80% RH, the curve increases with time at first and then begins to oscillate in a size range where a lot of spikes can be seen. The ascending from the bottom to the peak of a spike means that the largest droplet in the view area is growing over time, while the drop from the peak to the bottom means that the largest droplet leaves the surface. Fig. 8(b) shows the average, the maximum, and the minimum value of the oscillation range against humidity in terms of subcooling. It can be seen that the oscillation center (average value) moves up with increasing subcooling degree, though the changing degree is relatively small when the subcooling is larger than 4^{o}C. The amplitude of the oscillation range becomes larger in the highly humid condition, which suggests that large drops are more likely to be formed in the highly humid air. The maximum diameter oscillating within a certain range rather than continuously increasing further validates our hypothesis.

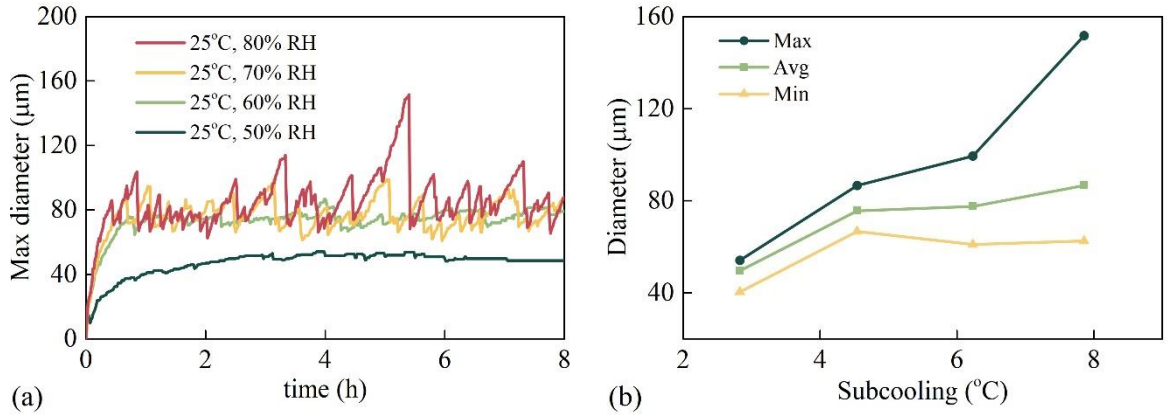

Fig. 8. (a) The maximum diameter under condition A1 - A4. (b) The maximum, the average, and the minimum value of the maximum diameter in the oscillation range.

The condensate image of V2 captured at each hour under condition A4 is shown in Fig. 9. It can be seen from the figure that the distribution of condensate drops at different times seems similar in visual. To quantitively investigate the condensate droplets size distribution, the diameter of condensate drops was analyzed using Trainable Weka Segmentation Tool. Droplets with a diameter smaller than 15 μm were ignored to improve image processing accuracy. The histogram of droplets diameter at each hour is illustrated in Fig. 10. In the figure, a class of 25 μm and a diameter range of 12.5 μm – 162.5 μm was chosen to account for the frequency of droplets with different sizes. To make the number of droplets at different time groups more comparable, each frequency was normalized by its largest frequency in each time group to work out the normalized diameter distribution curve, which is also illustrated in Fig. 10 and represented by the right Y-axis. From the figure, it can be seen that there is a similar diameter distribution curve for condensate droplets at different times. Most droplets have a size between 12.5 μm and 37.5 μm. The number of droplets with a diameter larger than 100 μm decreases to near zero, which indicates that most droplets disappeared from the view area before growing larger than the size of 100 μm.

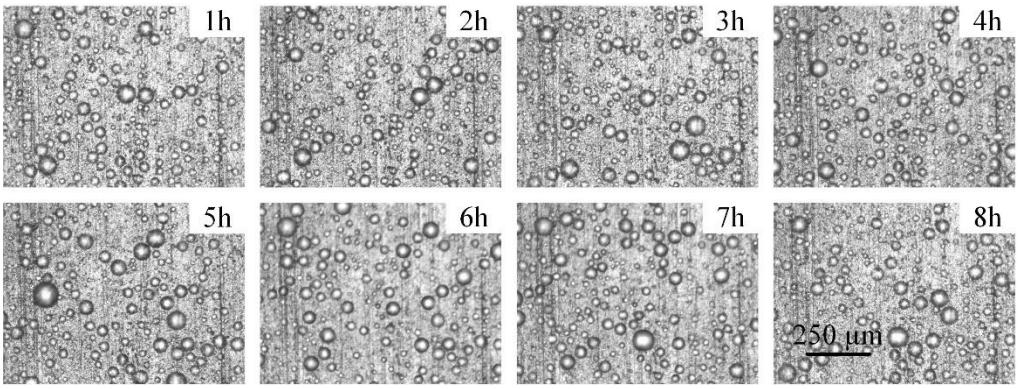

Fig. 9. Condensate image of the view area V2 under condition A4.

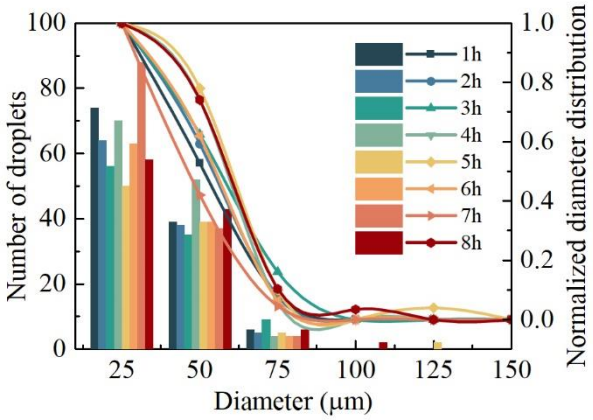

Fig. 10. The diameter distribution of condensate droplets under condition A4.

3.4 Condensate on the superhydrophobic aluminum sheet under various air change rates

Fig. 11 shows the condensate image of the view area V2 under various air change rates (condition B1 – B4). It can be seen from the figure that the differences in the condensate are relatively small under different air change rates compared with different humidity conditions. However, the condensate image clearly shows that the droplets formed in certain positions are significantly larger than the surrounding droplets, which has been demonstrated in the previous section. A similar phenomenon occurring repeatedly under various conditions means that large droplets appearing at these positions may not be occasional, but related to the properties of the material surface structures, which will be discussed in the next section.

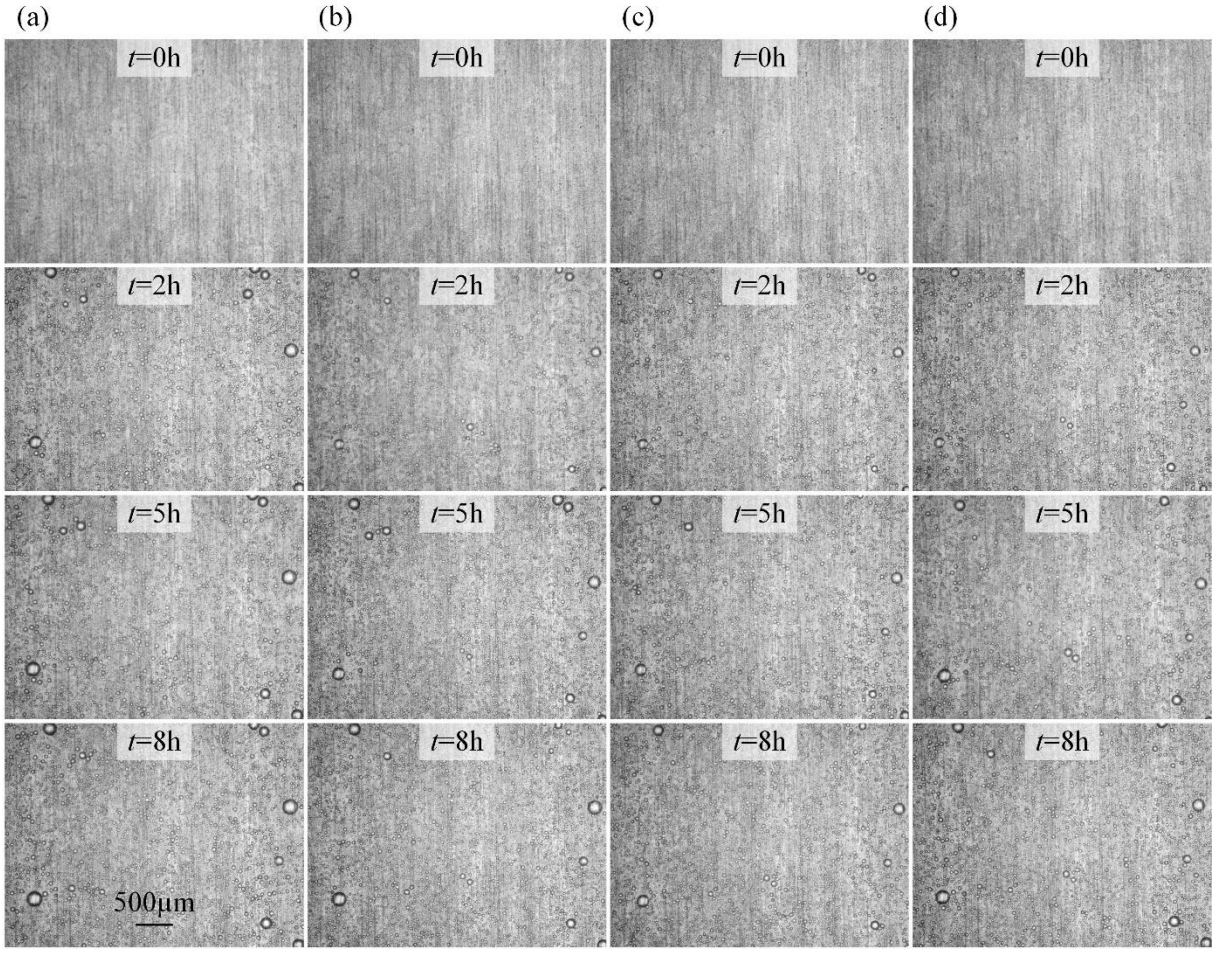

Fig. 11. The condensate image of the view area V1 under various air change rates at 25ºC, 60% RH: (a) 0 ACH. (b) 3.1 ACH. (c) 5.9 ACH. (d) 9 ACH.

The condensate image of the view area V2 under various air change rates is shown in Fig. 12. There are no large droplets appearing in the view area during experiments, which is again in line with our hypothesis. The maximum diameter of the view area V2 under various air change rates is shown in Fig. 13. For each maximum diameter curve, it increases with time firstly and then oscillates in a certain range rather than continuously increasing. The difference of the maximum diameter curve between different air change rates is relatively small, unlike that under different humidity conditions. That possibly because local air velocity near the radiant cooled ceiling panel surface are close for different air change rates.

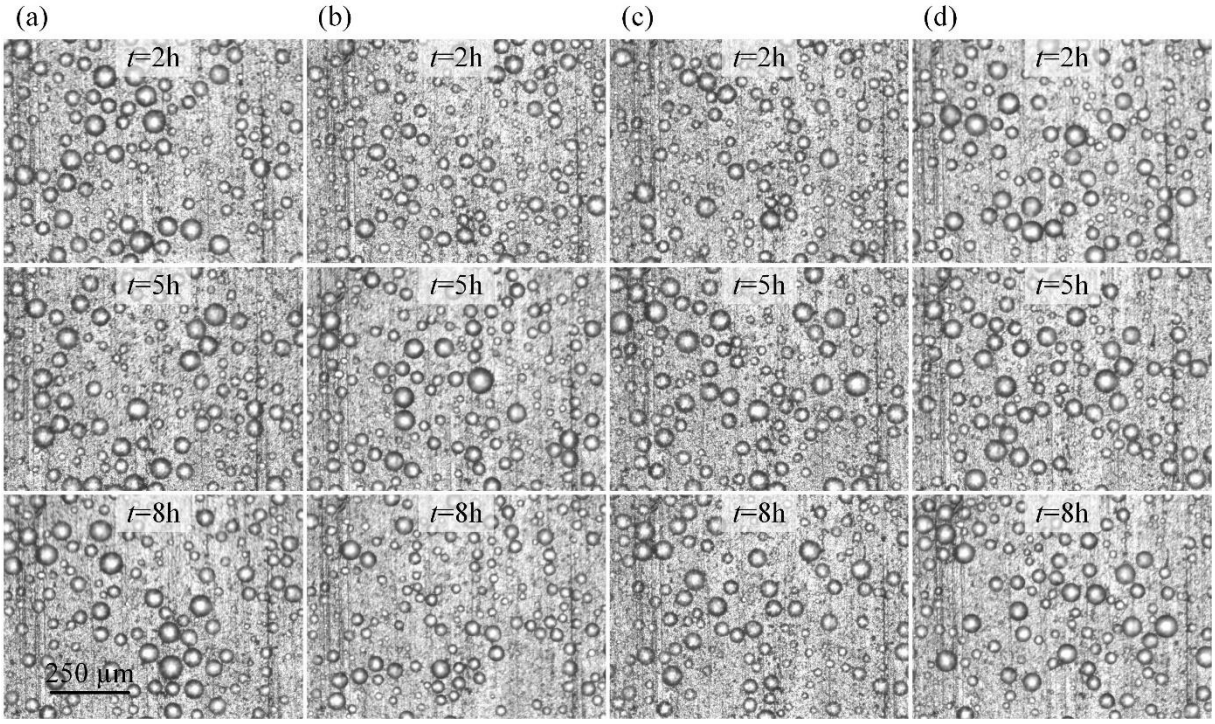

Fig. 12. The condensate image of the view area V2 under various air change rates at 25ºC, 60% RH: (a) 0 ACH. (b) 3.1 ACH. (c) 5.9 ACH. (d) 9 ACH.

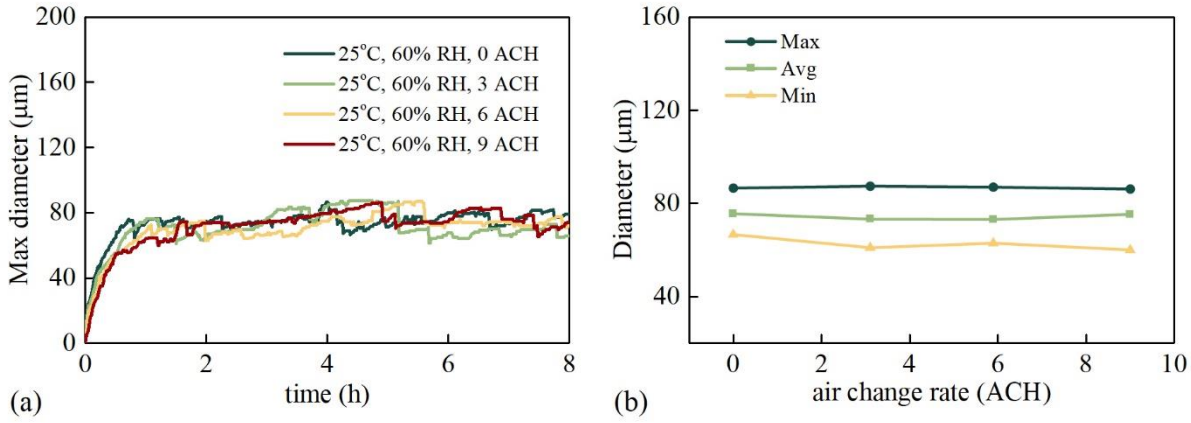

Fig. 13. (a) The maximum diameter under conditions B1 - B4. (b) The maximum, the average, and the minimum value of the maximum diameter in the oscillation range.

3.5 Condensate on the pure aluminum sheet

The condensate on the pure aluminum sheet under condition A4 is shown in Fig. 14. Different to the superhydrophobic surface, drops on the pure aluminum sheet grew continuously hour by hour, and finally, the largest drop with a diameter near 4 mm was formed.

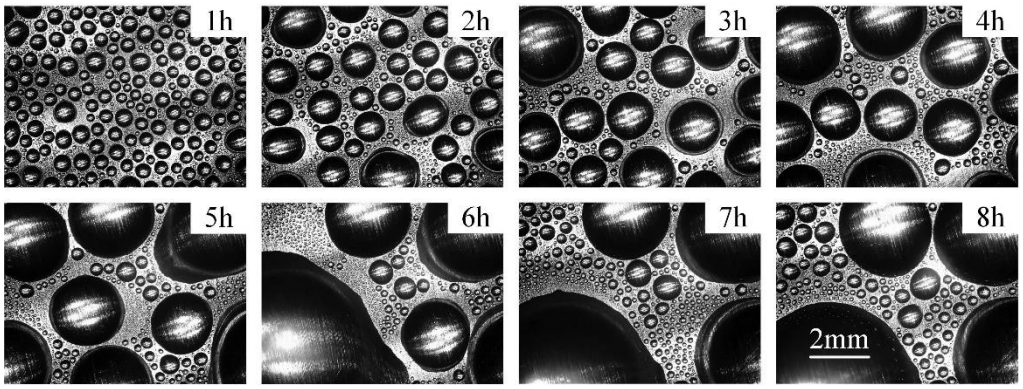

Fig. 14. The image of condensate drops on the pure aluminum sheet under condition A4.

The diameter of the largest droplet in the view area V2 of the superhydrophobic and on the pure aluminum sheet under condition A4 in relation to the condensation time is shown in Fig. 15. The vertical axis is scaled as logarithmic since there is a difference of two orders of magnitude between the size of droplets on two samples. The maximum diameter is analyzed based on the condensate image of V2 captured per minute for the superhydrophobic aluminum sheet, while the maximum diameter was measured based on the condensate image captured per ten minutes for the pure aluminum sheet because the change of droplet size is relatively slow. It can be seen from the figure that the maximum diameter of droplets on the superhydrophobic aluminum sheet oscillates between 60 μm and 100 μm after increasing to this range, except for the time during 5 h and 5.5 h when the diameter grows from 100 μm to the peak value of approximately 150 μm. However, the maximum diameter of droplets on the pure aluminum sheet keeps increasing. In the first hour, the maximum diameter continuous to increase over time, but after that, it begins to increase step by step. This is because at the beginning a droplet grows through both the condensate water and the coalescence with neighbor droplets, but when the droplet grows larger, the influence of the condensate water becomes fewer since the condensate rate becomes smaller due to the increased thermal resistance between the vapor and the cooled surface. At this stage, a droplet grows slowly and steadily through condensate water before coalescing with neighbor droplets, but after a coalescence, the size of the coalesced droplet suddenly increases, resulting in the step change of the maximum diameter.

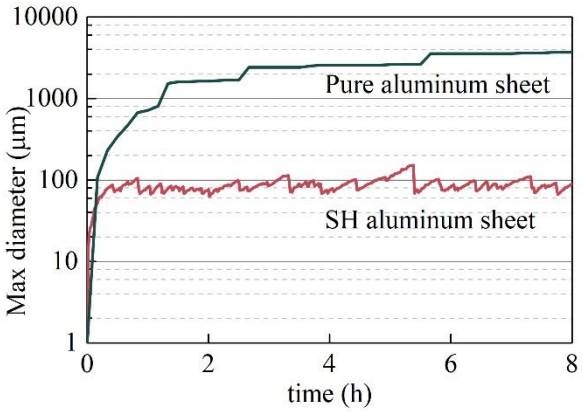

Fig. 15. The maximum diameter on the pure aluminum sheet and the superhydrophobic aluminum sheet under condition A4.

4 Discussion

4.1 The relation between the emergence of large drops and local microstructures.

Droplets coalescence and jumping are unique phenomena on the superhydrophobic surface due to the conversion from surface energy to kinetic energy. In this work, a majority of droplets coalescence and jump off before their diameters reach to 100 μm. It indicates that our superhydrophobic surface contributes to droplets detachment. However, when humidity is increased, nucleation and growing of several droplets appear at specific locations. That because Cassie-Wenzel transition of droplets occurred on hierarchical structures due to the increasing nucleation density [36]. Droplets will penetrate into nanostructures and remove the inside air, resulting in high adhesion force between droplets and substrate, followed by the continuous growth of droplets. This transition can be suppressed by tuning the feature size of superhydrophobic structures. For instance, a higher pillar height will increase the free-energy barrier resulting in a more difficult transition from Cassie state to Wenzel state [37]. However, the tunable and regular nanostructures fabricated by photolithography or laser machines are suitable for scientific research rather than industrial applications. In this work, we balance the cost and performance by chemical etching on aluminum sheets. It is still a great challenge to fabricate a superhydrophobic surface with rational feature size to suppress Cassie-Wenzel transition by low-cost methods. Moreover,

further investigations of the relation between humidity and condensation type on micro-nanostructures would have significance in various supercooled applications.

4.2 Droplet size vs sensory threshold

The condensation risk for occupants can be evaluated by their perception of the condensate. Tang et al [32] performed a sensory investigation of people by dripping tiny droplets to the forearm of subjects to find the sensible threshold of the droplet size. The investigation found a fuzzy range of droplet size with a radius ranging from 250 μm to 400 μm between the sensible and insensible stimuli. The average sensory threshold in terms of the radius of droplets was 325 μm, or 650 μm in terms of diameter.

In addition to the tactile perception, the visual perception of droplets should also be considered, that is because visible droplets on ceilings may strengthen occupants' concern on dripping risks. The visible threshold of drops is evaluated by people's vision acuity. A normal vision acuity in Snellen Chart is 6/6 meters, which means a man needs to discriminate two contours separated by 1 arc minute [38]. A theoretical angular resolution of a normal eye with a given pupil diameter of 2.4 mm and wavelength of light of 560 nm is 0.98 arc minute [39], which is similar to the above value. So, the angular resolution of 1 arc minute is used to calculate the spatial resolution. Since the ceiling is about 1 meter away from occupants standing in the room, the diameter of the minimum droplet on the ceiling people can see is about 291 μm.

Table 4 shows the diameter of the largest droplet in view area V1 and V2 during the eight-hour condensation experiment under conditions A1 – A4. The largest droplet in the view area V1 is 802.5 μm. The size is larger than the sensory threshold of 650 μm. For the view area V2, the diameter of the largest droplet is 151.7 μm, which is smaller than the visual threshold of people. The result indicates that the size of condensate drops in the area where droplets can detach through coalescence-induced jumping motion can be well limited below the perception threshold of people.

Table 4

The diameter of the largest droplet in the view area V1 and V2 under condition A1 – A4.

View area	Condition	Maximum diameter (μm)
V1	A1	108.3
	A2	222.9
	A3	544.6
	A4	802.5
V2	A1	54.1
	A2	86.7
	A3	99.4
	A4	151.7
Sensory threshold: 650 μm		

4.3 Cooling capacity

A radiant cooling panel with superhydrophobic surface can be operated with a temperature lower than the air dew point, which means the indoor air could be dehumidified by the panel. The condensate water droplets will detach from the surface and bump into the indoor air through the coalescence-induced jumping motion. If the jumping droplets were transported out of the room by ventilation systems, then the total moisture in the room will be reduced and the indoor air will be dehumidified.

The total cooling capacity of a superhydrophobic radiant cooling panel includes the latent cooling capacity and the sensible cooling capacity. The latent cooling capacity is related to the condensate rate between indoor air and the superhydrophobic surface. The sensible cooling capacity depends on the convection heat transfer rate and the radiation heat transfer rate between the superhydrophobic panel and room. In general, the cooling capacity of the superhydrophobic radiant cooling panel operated below the air dew point should be larger than conventional radiant cooling panels because of the lower operating temperature, but there are some differences in heat transfer mechanism. First, the convection heat transfer and the absorption of thermal radiation of the cooling surface can be affected by the condensate layer. Secondly, the detached tiny droplets that jump into the indoor air may bring some sensible cooling effects to the indoor air through evaporation processes.

5 Conclusion

Condensation is one of the factors that limit the application of radiant cooling systems. The anti-condensation potential of the superhydrophobic surface materials provides possibilities for mitigating the condensation risk of radiant cooling systems. In this study, a superhydrophobic aluminum sheet was used to perform the condensation experiment under typical indoor conditions for a series of eight-hour periods. The findings of the study are concluded as follows:

- The largest drop that appeared in the high humidity conditions had a diameter of 802.5 μm in the observed area of 4.08 mm x 3.06 mm in size. Increased number of large drops can be seen with increasing humidity. Some large drops always appeared in the same positions under different experimental conditions, which may be related to the microstructure of the superhydrophobic surface.
- In a focused small area of 0.96 mm x 0.72 mm in size on the superhydrophobic aluminum sheet, the diameter of the largest drop firstly increased with time and then oscillated in a range rather than increasing continuously; and the diameter of the largest drop under the high humidity condition was 151.7 μm. This value was smaller than people's sensory threshold and visual threshold.
- Condensation experiments were performed under different humidity conditions and air change rates. The results indicated that the size of the largest drop formed increased with increasing humidity, but the effects of the air change rate on the droplet size were not obvious.
- In comparison, the size of condensate drops on the untreated aluminum sheet surface kept increasing against condensation time, and the diameter of the largest drop in the observed area grew up to 4 mm.

The results of this study provide encouraging experimental evidence that the size of condensate droplets on the superhydrophobic surface can be limited below people's perceptional threshold during in a typical eight-hour operation period. It can be deduced that when this happens, a cooled-ceiling panel surface can work at a temperature up to 8^{o}C below the room dew-point temperature, and thus the cooling capacity of a radiant cooling panel can be significantly increased, enhanced with the condensation heat

release process. However, the non-uniformity of the surface nano-structures on the superhydrophobic surface can lead to the appearance of some unwanted large droplets. More research is needed to further study the scalability, durability, uniformity, and the overall condensation performance of superhydrophobic materials under a wider range of conditions.

CRediT authorship contribution statement

Zhong Ziwen: Methodology, Investigation, Formal analysis, Data Curation, Visualization, Writing - Original Draft.

Niu Jianlei: Conceptualization, Methodology, Resources, Funding acquisition, Supervision, Writing - Review & Editing.

Ma Wei: Investigation, Formal analysis, Visualization, Writing - Original Draft.

Yao Shuhuai: Resources, Supervision, Conceptualization, Methodology, Funding acquisition.

Yang Meng: Resources, Methodology.

Wang Zuankai: Resources, Supervision, Conceptualization, Methodology, Funding acquisition.

Acknowledgements

This work was fully supported by the General Research Funding of Research Grant Council of the Hong Kong SAR, China (Project No. 15206620).

References

[1] Hong Kong Energy Statistics, in, Census and Statistics Department, Hong Kong SAR, 2019.
[2] Hong Kong Energy End-use Data, in, Electrical and Mechanical Service Department, The Goverment of Hong Kong SAR, Hong Kong SAR, 2019.
[3] Y. Xu, V. Ramanathan, D.G. Victor, Global warming will happen faster than we think, Nature, 564 (7734) (2018) 30-32.
[4] N. Watts, M. Amann, N. Arnell, S. Ayeb-Karlsson, K. Belesova, M. Boykoff, P. Byass, W. Cai, D. Campbell-Lendrum, S. Capstick, J. Chambers, C. Dalin, M. Daly, N. Dasandi, M. Davies, P. Drummond, R. Dubrow, K.L. Ebi, M. Eckelman, P. Ekins, L.E. Escobar, L. Fernandez Montoya, L. Georgeson, H. Graham, P. Haggar, I. Hamilton, S. Hartinger, J. Hess, I. Kelman, G. Kiesewetter, T. Kjellstrom, D. Kniveton, B. Lemke, Y. Liu, M. Lott, R. Lowe, M.O. Sewe, J. Martinez-Urtaza, M. Maslin, L. McAllister, A. McGushin, S. Jankin Mikhaylov, J. Milner, M. Moradi-Lakeh, K. Morrissey, K. Murray,

S. Munzert, M. Nilsson, T. Neville, T. Oreszczyn, F. Owfi, O. Pearman, D. Pencheon, D. Phung, S. Pye, R. Quinn, M. Rabbaniha, E. Robinson, J. Rocklöv, J.C. Semenza, J. Sherman, J. Shumake-Guillemot, M. Tabatabaei, J. Taylor, J. Trinanes, P. Wilkinson, A. Costello, P. Gong, H. Montgomery, The 2019 report of The Lancet Countdown on health and climate change: ensuring that the health of a child born today is not defined by a changing climate, The Lancet, 394 (10211) (2019) 1836-1878.
[5] K.-N. Rhee, B.W. Olesen, K.W. Kim, Ten questions about radiant heating and cooling systems, Building and Environment, 112 (2017) 367-381.
[6] J. Niu, J. Kooi, H. Rhee, Energy saving possibilities with cooled-ceiling systems, Energy and buildings, 23 (2) (1995) 147-158.
[7] S.A. Mumma, Chilled ceiling condensation control, ASHRAE IAQ Applications, 4 (4) (2003) 22-23.
[8] S.A. Mumma, Chilled ceilings in parallel with dedicated outdoor air systems: Addressing the concerns of condensation, capacity, and cost, ASHRAE Transactions, 108 (2002) 220.
[9] K.M. Shank, S.A. Mumma, Selecting the supply air conditions for a dedicated outdoor air system working in parallel with distributed sensible cooling terminal equipment/Discussion, ASHRAE Transactions, 107 (2001) 562.
[10] J. Niu, L. Zhang, H. Zuo, Energy savings potential of chilled-ceiling combined with desiccant cooling in hot and humid climates, Energy and buildings, 34 (5) (2002) 487-495.
[11] J. Niu, L. Zhang, H. Zuo, Analysis of energy and humidity performance of a system combining chilled ceiling with desiccant cooling, ASHRAE transactions, 108 (2002) 195.
[12] A. Binghooth, Z. Zainal, Performance of desiccant dehumidification with hydronic radiant cooling system in hot humid climates, Energy and Buildings, 51 (2012) 1-5.
[13] K. Zhao, X.-H. Liu, T. Zhang, Y. Jiang, Performance of temperature and humidity independent control air-conditioning system in an office building, Energy and Buildings, 43 (8) (2011) 1895-1903.
[14] A. Ameen, K. Mahmud, Desiccant Dehumidification with Hydronic Radiant Cooling System for Air-Conditioning Applications in Humid Tropical Climates, ASHRAE transactions, 111 (2) (2005).
[15] D. Song, T. Kim, S. Song, S. Hwang, S.-B. Leigh, Performance evaluation of a radiant floor cooling system integrated with dehumidified ventilation, Applied Thermal Engineering, 28 (11-12) (2008) 1299-1311.
[16] X. Hao, G. Zhang, Y. Chen, S. Zou, D.J. Moschandreas, A combined system of chilled ceiling, displacement ventilation and desiccant dehumidification, Building and Environment, 42 (9) (2007) 3298-3308.
[17] P. Navid, S. Niroomand, C.J. Simonson, An analytical model for predicting frosting limit in membranes, International Journal of Refrigeration, 99 (2019) 316-326.
[18] M. Hout, N. Ghaddar, K. Ghali, N. Ismail, M. Simonetti, G.V. Fracastoro, J. Virgone, A. Zoughaib, Displacement ventilation with cooled liquid desiccant dehumidification membrane at ceiling; modeling and design charts, Energy, 139 (Supplement C) (2017) 1003-1015.
[19] M. Muslmani, N. Ghaddar, K. Ghali, Performance of combined displacement ventilation and cooled ceiling liquid desiccant membrane system in Beirut climate, Journal of Building Performance Simulation, 9 (6) (2016) 648-662.
[20] D. Xing, N. Li, H. Cui, L. Zhou, Q. Liu, Theoretical study of infrared transparent cover preventing condensation on indoor radiant cooling surfaces, Energy, 201 (2020) 117694.
[21] E. Teitelbaum, K.W. Chen, D. Aviv, K. Bradford, L. Ruefenacht, D. Sheppard, M. Teitelbaum, F. Meggers, J. Pantelic, A. Rysanek, Membrane-assisted radiant cooling for expanding thermal comfort zones globally without air conditioning, Proceedings of the National Academy of Sciences of the United States of America, (2020).
[22] E. Teitelbaum, A. Rysanek, J. Pantelic, D. Aviv, S. Obelz, A. Buff, Y. Luo, D. Sheppard, F. Meggers, Revisiting radiant cooling: condensation-free heat rejection using infrared-transparent enclosures of chilled panels, Architectural Science Review, 62 (2) (2019) 152-159.
[23] X.-M. Li, D. Reinhoudt, M. Crego-Calama, What do we need for a superhydrophobic surface? A review on the recent progress in the preparation of superhydrophobic surfaces, Chemical Society Reviews, 36 (8) (2007) 1350-1368.
[24] D. Wang, Q. Sun, M.J. Hokkanen, C. Zhang, F.-Y. Lin, Q. Liu, S.-P. Zhu, T. Zhou, Q. Chang, B. He, Q. Zhou, L. Chen, Z. Wang, R.H.A. Ras, X. Deng, Design of robust superhydrophobic surfaces, Nature, 582 (7810) (2020) 55-59.

[25] M. He, Y. Ding, J. Chen, Y. Song, Spontaneous Uphill Movement and Self-Removal of Condensates on Hierarchical Tower-like Arrays, ACS Nano, 10 (10) (2016) 9456-9462.
[26] N. Miljkovic, R. Enright, Y. Nam, K. Lopez, N. Dou, J. Sack, E.N. Wang, Jumping-Droplet-Enhanced Condensation on Scalable Superhydrophobic Nanostructured Surfaces, Nano Letters, 13 (1) (2013) 179-187.
[27] X. Chen, J. Wu, R. Ma, M. Hua, N. Koratkar, S. Yao, Z. Wang, Nanograssed Micropyramidal Architectures for Continuous Dropwise Condensation, Advanced Functional Materials, 21 (24) (2011) 4617-4623.
[28] J.B. Boreyko, C.-H. Chen, Self-Propelled Dropwise Condensate on Superhydrophobic Surfaces, Physical Review Letters, 103 (18) (2009) 184501.
[29] C.-H. Chen, Q. Cai, C. Tsai, C.-L. Chen, G. Xiong, Y. Yu, Z. Ren, Dropwise condensation on superhydrophobic surfaces with two-tier roughness, Applied Physics Letters, 90 (17) (2007) 173108.
[30] J. Feng, Y. Pang, Z. Qin, R. Ma, S. Yao, Why Condensate Drops Can Spontaneously Move Away on Some Superhydrophobic Surfaces but Not on Others, ACS Applied Materials & Interfaces, 4 (12) (2012) 6618-6625.
[31] Y. Hou, Y. Shang, M. Yu, C. Feng, H. Yu, S. Yao, Tunable Water Harvesting Surfaces Consisting of Biphilic Nanoscale Topography, ACS Nano, 12 (11) (2018) 11022-11030.
[32] H. Tang, X.-H. Liu, H. Li, Y. Zhou, Y. Jiang, Study on the reduction of condensation risks on the radiant cooling ceiling with superhydrophobic treatment, Building and Environment, 100 (2016) 135-144.
[33] W. Ma, Y. Li, C.Y.H. Chao, C.Y. Tso, B. Huang, W. Li, S. Yao, Solar-assisted icephobicity down to −60°C with superhydrophobic selective surfaces, Cell Reports Physical Science, 2 (3) (2021) 100384.
[34] J. Schindelin, I. Arganda-Carreras, E. Frise, V. Kaynig, M. Longair, T. Pietzsch, S. Preibisch, C. Rueden, S. Saalfeld, B.J.N.m. Schmid, Fiji: an open-source platform for biological-image analysis, Nature Methods, 9 (7) (2012) 676-682.
[35] I. Arganda-Carreras, V. Kaynig, C. Rueden, K.W. Eliceiri, J. Schindelin, A. Cardona, H.J.B. Sebastian Seung, Trainable Weka Segmentation: a machine learning tool for microscopy pixel classification, Bioinformatics, 33 (15) (2017) 2424-2426.
[36] M.D. Mulroe, B.R. Srijanto, S.F. Ahmadi, C.P. Collier, J.B. Boreyko, Tuning superhydrophobic nanostructures to enhance jumping-droplet condensation, ACS nano, 11 (8) (2017) 8499-8510.
[37] T. Koishi, K. Yasuoka, S. Fujikawa, T. Ebisuzaki, X.C. Zeng, Coexistence and transition between Cassie and Wenzel state on pillared hydrophobic surface, Proceedings of the National Academy of Sciences, 106 (21) (2009) 8435-8440.
[38] E.S. Perkins, H. Davson, in: Human eye. Encyclopedia Britannica, 2020.
[39] M. Yanoff, J.S. Duker, Ophthalmology, 3rd ed., Mosby Elsevier, Philadelphia, 2009.